

Large-scale clustering as a probe of the origin and the host environment of fast radio bursts

Masato Shirasaki

*National Astronomical Observatory of Japan, Mitaka, Tokyo 181-8588, Japan**

Kazumi Kashiyama

Department of Physics, University of Tokyo, Tokyo 113-0033, Japan †

Naoki Yoshida

*Department of Physics, University of Tokyo, Tokyo 113-0033, Japan
Kavli Institute for the Physics and Mathematics of the Universe (WPI),
University of Tokyo, Kashiwa, Chiba 277-8583, Japan and*

CREST, Japan Science and Technology Agency, 4-1-8 Honcho, Kawaguchi, Saitama, 332-0012, Japan ‡

We propose to use degree-scale angular clustering of fast radio bursts (FRBs) to identify their origin and the host galaxy population. We study the information content in autocorrelation of the angular positions and dispersion measures (DM) and in cross-correlation with galaxies. We show that the cross-correlation with Sloan Digital Sky Survey (SDSS) galaxies will place stringent constraints on the mean physical quantities associated with FRBs. If $\sim 10,000$ FRBs are detected with \lesssim deg resolution in the SDSS field, the clustering analysis with the intrinsic DM scatter of 100 pc/cm^3 can constrain the global abundance of free electrons at $z \lesssim 1$ and the large-scale bias of FRB host galaxies (the statistical relation between the distribution of host galaxies and cosmic matter density field) with fractional errors (with a 68% confidence level) of $\sim 10\%$ and $\sim 20\%$, respectively. The mean near-source dispersion measure and the delay time distribution of FRB rates relative to the global star forming rate can be also determined by combining the clustering and the probability distribution function of DM. Our approach will be complementary to high-resolution (\ll deg) event localization using e.g., VLA and VLBI for identifying the origin of FRBs and the source environment. We strongly encourage future observational programs such as CHIME, UTMOST, and HIRAX to survey FRBs in the SDSS field.

I. INTRODUCTION

Fast radio bursts (FRBs) are millisecond transients at \sim GHz frequencies characterized by their large dispersion measure (DM) of an order of 1000 pc cm^{-3} [1–9]. If the DMs are mainly due to intergalactic propagation [10, 11], FRBs are cosmological events at redshifts of $0.3 - 1.3$. Although various models have been proposed, e.g., [2, 12–16], the origin is still uncertain.

Recently, Refs [17, 18] succeeded in localizing a repeating FRB 121102 with a submilliarcsecond resolution using the Karl G. Jansky Very Large Array (VLA) and the European Very Long Baseline Array Interferometry (VLBI). The host galaxy was identified as a dwarf star-forming galaxy at $z = 0.19$ [19], confirming that the FRB source is at a cosmological distance. Furthermore, a possible persistent radio counterpart was identified for FRB 121102 [17, 18]. Such a precise localization is a direct way to probe the physical properties of FRB sources and their environment and will be effective especially for repeating bursts. As for nonrepeating FRB, a blind survey using VLA will be time consuming to localize one event (see Ref [20]).

Upcoming FRB surveys with e.g., CHIME, UTMOST [21], and HIRAX [22] will be able to detect $\sim 10,000$ FRBs per decade. Although the host galaxies cannot be directly identified with the \sim arcmin angular resolution, such a large number of FRBs can be used to probe the global abundance and spatial distribution of missing baryons [10, 11, 23, 24], physical properties of intergalactic medium (IGM) [25], and three-dimensional clustering of large-scale structure [26]. It is important to develop frameworks for statistical analyses.

In this paper, we propose to use large-scale (\sim deg) clustering of FRBs to study the statistical information of the host environment. In addition to autocorrelation analysis of FRB observables such as sky locations and DMs [26], we consider cross-correlation analysis with Sloan Digital Sky Survey (SDSS) galaxies. By doing this, properties of FRB host galaxies, e.g., redshift distribution and clustering bias, can be statistically determined. Furthermore, the cross-correlation can be used to infer the mean value and scatter of the DM contribution from FRB host galaxies, which can then be used to distinguish different models for FRBs.

The rest of the paper is organized as follows. In Sec. II, we summarize FRB observables and their possible clustering properties. We present a theoretical model of the FRB autocorrelation in Sec. II B, and the cross-correlation with galaxies in Sec. II C. The expected signal-to-noise ratio (S/N) of the correlations are derived

* masato.shirasaki@nao.ac.jp

† kashiyama@phys.s.u-tokyo.ac.jp

‡ naoki.yoshida@ipmu.jp

in Sec. IID. In Sec. III, we perform a Fisher analysis to study possible constraints obtained from the clustering analyses. We also study how the constraints can be improved by combining another statistic of FRBs, i.e., probability distribution function of DM, in Sec. IIIA. Concluding remarks and discussions are given in Sec. IV. Throughout the paper, we adopt the standard Λ CDM model with the following parameters; $\Omega_{\text{m}0} = 0.315$, $\Omega_{\Lambda} = 0.685$, $\sigma_8 = 0.831$, $w_0 = -1$, $h = 0.672$ and $n_s = 0.964$, which are consistent with the PLANCK 2015 results [27].

II. LARGE-SCALE CLUSTERING

A. FRB Observables

In this paper, we consider the dispersion measure DM_{obs} and angular position $\boldsymbol{\theta}$ as observables of FRB¹.

Angular number density of sources

For a given three-dimensional source distribution $n_s(\boldsymbol{\theta}, z)$, the angular number density $n_{s,2\text{D}}(\boldsymbol{\theta})$ can be computed as

$$n_{s,2\text{D}}(\boldsymbol{\theta}) = \int_0^{\infty} dz \frac{\chi^2(z)}{H(z)(1+z)} n_s(\boldsymbol{\theta}, z), \quad (1)$$

where z is the redshift, $\chi(z)$ is the comoving distance, and $H(z)$ is the Hubble parameter. The factor of $1+z$ in Eq. (1) accounts for the effect of cosmological time dilation. The average projected number density is then given by

$$\bar{n}_{s,2\text{D}} = \int_0^{\infty} dz \frac{\chi^2(z)}{H(z)(1+z)} \bar{n}_s(z), \quad (2)$$

where $\bar{n}_s(z)$ is the average comoving number density of sources at the redshift of z . From Eqs. (1) and (2), one can define the angular over-density field as

$$\begin{aligned} \delta_{s,2\text{D}}(\boldsymbol{\theta}) &\equiv \frac{n_{s,2\text{D}}(\boldsymbol{\theta})}{\bar{n}_{s,2\text{D}}} - 1, \\ &= \int_0^{\infty} dz W_s(z) \delta_s(\boldsymbol{\theta}, z), \end{aligned} \quad (3)$$

$$W_s(z) = \frac{1}{\bar{n}_{s,2\text{D}}} \frac{\chi^2(z)}{H(z)(1+z)} \bar{n}_s(z). \quad (4)$$

¹ We note that the polarization and pulse profile are also important observables, from which the magnetic field and turbulent motion of gas in the line-of-sight can be inferred, respectively [8]. To this end, however, the signal-to-noise ratio (S/N) of the FRB should be high, and detection rate of such events will be limited.

As a fiducial model, we assume that $\bar{n}_s(z)$ follows the star-formation history $\dot{\rho}_*(z)$ as

$$\bar{n}_s(z) = \mathcal{A} \dot{\rho}_*(z) \exp \left[-\frac{d_L^2(z)}{2d_L^2(z_{\text{cut}})} \right], \quad (5)$$

where $d_L(z)$ is the luminosity distance, the exponential form represents an instrumental S/N threshold, and \mathcal{A} is determined by the normalization of Eq. (2). The star-formation history can be parametrized as [28, 29]

$$\dot{\rho}_*(z) \propto \frac{\alpha_0 + \alpha_1 z}{1 + (z/\alpha_2)^{\alpha_3}}, \quad (6)$$

with $\alpha_0 = 0.0170$, $\alpha_1 = 0.13$, $\alpha_2 = 3.3$, and $\alpha_3 = 5.3$. Our fiducial model [Eq. (5)] is consistent with an estimated redshift distribution of the observed FRBs [30] if the redshift cutoff is set to be $z_{\text{cut}} = 0.5$ [31]. Note that our results are less sensitive to α_2 and α_3 since these parameters determine the redshift distribution at $z \gtrsim 2$. The dependence of z_{cut} on the clustering analysis is summarized in Sec. IID. There, we found that the choice of z_{cut} have a small impact on the signal-to-noise in auto-correlation of DM and the cross correlation of DM and galaxies. In Sec. III, we examine another model of \bar{n}_s taking into account a time delay of FRB rates relative to the global star-forming rate [see Eq. (45)].

Two-dimensional field of dispersion measures

$\text{DM}_{\text{obs}}(\boldsymbol{\theta})$ is defined as the integral of number density of free electrons along a line of sight, which can be decomposed as

$$\text{DM}_{\text{obs}} = \text{DM}_{\text{IGM}} + \text{DM}_{\text{host}} + \text{DM}_{\text{MW}}, \quad (7)$$

where DM_{IGM} , DM_{host} and DM_{MW} represent the contributions from the IGM, FRB host galaxies, and the Milky way, respectively. DM_{host} includes the interstellar medium of the host and near-source plasma. We assume that $\text{DM}_{\text{MW}}(\boldsymbol{\theta})$ for each direction is already determined from Galactic pulsar observations [32] and can be subtracted from $\text{DM}_{\text{obs}}(\boldsymbol{\theta})$ ². In the following, we focus on the extragalactic DM field expressed as $\text{DM}_{\text{ext}} = \text{DM}_{\text{IGM}} + \text{DM}_{\text{host}}$.

For a fixed source redshift z_s , DM_{IGM} is given by

$$\text{DM}_{\text{IGM}}(\boldsymbol{\theta}, z_s) = \int_0^{z_s} dz \frac{n_e(\boldsymbol{\theta}, z)}{H(z)(1+z)^2}, \quad (8)$$

² In real, the subtraction of DM_{MW} is still uncertain and the imperfect subtraction can affect the measurement of the autocorrelation of DM. On the other hand, the cross-correlation analysis of DM with extragalactic objects should be insensitive to the subtraction of galactic DM, since the galactic DM does not correlate with the spatial distributions of extragalactic objects. As we show in the following sections, the cross correlation of DM and galaxies can play a central role to constrain the parameters of FRB sources, indicating that the imperfect subtraction will not affect our results significantly.

where $n_e(\boldsymbol{\theta}, z)$ represents the three-dimensional number density of free electrons at redshift z . The average density of IGM electrons can be expressed as [25, 33]

$$\bar{n}_e(z) = n_0(1+z)^3 f_e(z), \quad (9)$$

where

$$n_0 = \frac{\Omega_b \rho_{\text{crit},0}}{m_H} = 2.475 \times 10^{-7} \left(\frac{\Omega_b h^2}{0.022} \right) \text{cm}^{-3}, \quad (10)$$

with Ω_b being the baryon density normalized by the critical density $\rho_{\text{crit},0}$ at $z = 0$ and $h = H(z = 0)/(100 \text{ km/s/Mpc})$. Also,

$$f_e = \left[(1-Y)f_{\text{HII}} + \frac{1}{4}Y(f_{\text{HeII}} + 2f_{\text{HeIII}}) \right], \quad (11)$$

where $Y \simeq 0.25$ is the mass fraction of helium, f_{HII} is the ionization fraction of hydrogen, f_{HeII} and f_{HeIII} represent the ionization fractions of singly and doubly ionized helium, respectively. After helium reionization (occurred at $z \sim 2-3$), we can approximate as $f_{\text{HII}} = 1$, $f_{\text{HeII}} = 0$, and $f_{\text{HeIII}} = 1$. In this case, $f_e = 0.88$ and

$$\text{DM}_{\text{IGM}}(\boldsymbol{\theta}, z_s) = 1060 \text{ pc cm}^{-3} \left(\frac{f_e}{0.88} \right) \left(\frac{\Omega_b h^2}{0.022} \right) \left(\frac{h}{0.7} \right)^{-1} \times \left\{ \int_0^{z_s} dz \frac{(1+z)}{E(z)} [1 + \delta_e(\boldsymbol{\theta}, z_s)] \right\}, \quad (12)$$

where $E(z) = H(z)/H(z=0)$ and δ_e is the over-density field of free electrons. Note that Eq (12) with $\delta_e = 0$ correspond to Eq (2) in Ref [11], which is commonly used. The average DM_{IGM} for an angular position $\boldsymbol{\theta}$ can be described as

$$\text{DM}_{\text{IGM}}(\boldsymbol{\theta}) = \int_0^\infty dz W_{\text{DM,IGM}}(z) [1 + \delta_e(\boldsymbol{\theta}, z)], \quad (13)$$

where

$$W_{\text{DM,IGM}}(z) = 1060 \text{ pc cm}^{-3} \left(\frac{f_e}{0.88} \right) \left(\frac{\Omega_b h^2}{0.022} \right) \left(\frac{h}{0.7} \right)^{-1} \times \frac{(1+z)}{E(z)} \int_z^\infty W_s(z) dz. \quad (14)$$

We next consider the contribution from host galaxies. For galaxies at redshift of z_s , DM_{host} is expressed as

$$\text{DM}_{\text{host}}(\boldsymbol{\theta}, z_s) = \int d^2\theta_s \tau_e(\chi_s[\boldsymbol{\theta} - \boldsymbol{\theta}_s] | z_s) \times \bar{n}_s(z_s) [1 + \delta_s(\boldsymbol{\theta}_s, z_s)] \quad (15)$$

where $\chi_s = \chi(z_s)$ and $\tau_e(\mathbf{x}_\perp | z_s)$ represent the projected number density of free electrons around the host galaxy and the apparent angular size, respectively. In this paper, the apparent angular size of τ_e is assumed to be small enough, i.e. $\tau_e(\mathbf{x}, z) \propto \delta^{(2)}(\mathbf{x})$, where $\delta^{(2)}(\mathbf{x})$ is the two-dimensional delta function. This approximation should be reasonable when one considers the large-scale clustering of DM with angular separation of $\gtrsim 1$ deg. Taking

into account the source distribution, the average DM_{host} for an angular position $\boldsymbol{\theta}$ is given by

$$\text{DM}_{\text{host}}(\boldsymbol{\theta}) = \int_0^\infty dz W_{\text{DM,host}}(z) [1 + \delta_s(\boldsymbol{\theta}, z)], \quad (16)$$

where

$$W_{\text{DM,host}}(z) = \bar{\tau}_e(z) W_s(z). \quad (17)$$

In the above equation, $\bar{\tau}_e(z)$ represents the mean DM from galaxies at redshift of z . Note that $\bar{\tau}_e$ is considered to be averaged over the orientation and population of the host galaxies. The redshift dependence of $\bar{\tau}_e$ should contain the information of the environment of FRB sources, which is poorly known. In this paper, we assume $\bar{\tau}_e(z)$ to be constant, for simplicity. We take $\bar{\tau}_e = 100 \text{ pc cm}^{-3}$ as a face value, that is consistent with the observational constraint on the host galaxy of FRB 121102 [19].

According to Eqs (13) and (16), DM_{IGM} and DM_{host} can be expressed as the integral of over-density field of electron number density δ_e and source number density δ_s along a line of sight, respectively. In order to compute a possible clustering signal of these DMs, we adopt the linear bias model. In the linear bias model, a given over-density field δ_α is expressed as

$$\delta_\alpha(\mathbf{x}) = b_\alpha \delta_m(\mathbf{x}), \quad (18)$$

where δ_m represents the overdensity of cosmic matter density. In this model, the distribution of δ_α can be determined by δ_m , but the amplitude of their fluctuation is *biased* by a factor of b_α . The proportional factor b_α is referred to as the bias factor throughout this paper. The linear bias model is thought to be valid for the clustering analysis on large scales greater than $\sim 10 \text{ Mpc}$ [34].

B. FRB autocorrelation

We then consider the large-scale clustering of FRBs. In general, clustering information of a two-dimensional field $f(\boldsymbol{\theta})$ is encompassed in the two-point correlation function;

$$\xi_{ff}(\theta) = \langle f(\boldsymbol{\phi})f(\boldsymbol{\phi} + \boldsymbol{\theta}) \rangle - \langle f(\boldsymbol{\phi}) \rangle \langle f(\boldsymbol{\phi} + \boldsymbol{\theta}) \rangle. \quad (19)$$

The power spectrum $C_{ff}(\ell)$ defined as

$$C_{ff}(\ell) = \int d^2\theta \xi_{ff}(\theta) \exp(-i\boldsymbol{\ell} \cdot \boldsymbol{\theta}), \quad (20)$$

is commonly used in clustering analyses. Here $\ell = 2\pi/\theta$ is the multipole. In this paper, we adapt the flat-sky approximation.

Using Eqs. (3) and (4) with the Limber approximation [35], we can compute the angular power spectrum of the over-density field of FRB sources as

$$C_{ss}(\ell) = \int dz W_s^2(z) \frac{H(z)}{\chi^2(z)} \times b_{\text{FRB}}^2 P_m \left(\frac{\ell + 1/2}{\chi}, z \right), \quad (21)$$

where b_{FRB} is the bias factor of δ_s relative to the underlying matter over-density field δ_m and $P_m(k, z)$ represents the three-dimensional power spectrum of δ_m at redshift z . We assume that $P_m(k, z)$ is the linear matter power spectrum. The approximation of using linear matter power spectrum is valid at sufficiently large scales of $k \lesssim 0.1h/\text{Mpc}$. The linear matter power spectrum is computed with CAMB [36]. We also assume linear bias of $\delta_s(\boldsymbol{\theta}, z) = b_{\text{FRB}}\delta_m(\boldsymbol{\theta}, z)$ and compute the angular power spectrum of the extragalactic DM field DM_{ext} as

$$C_{\text{DM-DM}}(\ell) = C_{\text{IGM-IGM}}(\ell) + C_{\text{IGM-host}}(\ell) + C_{\text{host-host}}(\ell), \quad (22)$$

$$C_{\text{IGM-IGM}}(\ell) = \int dz W_{\text{DM,IGM}}^2(z) \frac{H(z)}{\chi^2(z)} \times b_e^2 P_m\left(\frac{\ell+1/2}{\chi}, z\right), \quad (23)$$

$$C_{\text{IGM-host}}(\ell) = \int dz 2W_{\text{DM,IGM}}(z)W_{\text{DM,host}}(z) \frac{H(z)}{\chi^2(z)} \times b_e b_{\text{FRB}} P_m\left(\frac{\ell+1/2}{\chi}, z\right), \quad (24)$$

$$C_{\text{host-host}}(\ell) = \int dz W_{\text{DM,host}}^2(z) \frac{H(z)}{\chi^2(z)} \times b_{\text{FRB}}^2 P_m\left(\frac{\ell+1/2}{\chi}, z\right), \quad (25)$$

where $b_e = \delta_e/\delta_m$ is the bias factor of electron density field.

Fig. 1 shows the auto power spectrum of DMs, $C_{\text{DM-DM}}$. Here we set $b_{\text{FRB}} = 1.3$, $b_e = 1$, and $\bar{\tau}_e = 100 \text{ pc cm}^{-3}$. Note that $b_{\text{FRB}} = 1.3$ is consistent with star-forming galaxies at $z \lesssim 1$ [37]. In this case, the clustering of IGM will dominate. We find that $C_{\text{IGM-host}}$ becomes larger than $C_{\text{IGM-IGM}}$ at $\ell = 100$ if $b_{\text{FRB}}\bar{\tau}_e \gtrsim 680 \text{ pc cm}^{-3}$. The dashed line in Fig. 1 represents the shot noise induced by the intrinsic scatter of DM around host galaxies $\sigma_{\text{DM,host}}$. The shot noise $N_{\text{DM-DM}}$ is computed as

$$N_{\text{DM-DM}} = \frac{\sigma_{\text{DM,host}}^2}{\bar{n}_{s,2\text{D}}} \quad (26)$$

$$= 1.95 (\text{pc cm}^{-3})^2 \left(\frac{\sigma_{\text{DM,host}}}{100 \text{ pc cm}^{-3}}\right)^2 \times \left(\frac{\bar{n}_{s,2\text{D}}}{1 \text{ deg}^{-2}}\right)^{-1}. \quad (27)$$

With a FRB number density of $\bar{n}_{2\text{D},s} \gtrsim 1 \text{ deg}^{-2}$, the signal $C_{\text{DM-DM}}$ is larger than the noise $N_{\text{DM-DM}}$ at $\ell \lesssim 100$ if $\sigma_{\text{DM,host}} \lesssim 100 \text{ pc cm}^{-3}$. We study the information content of $C_{\text{DM-DM}}$ in more detail in Sec. II D.

C. Cross-correlation with galaxies

The clustering analysis of the FRB autocorrelation can give some constraints on the model parameters of FRB

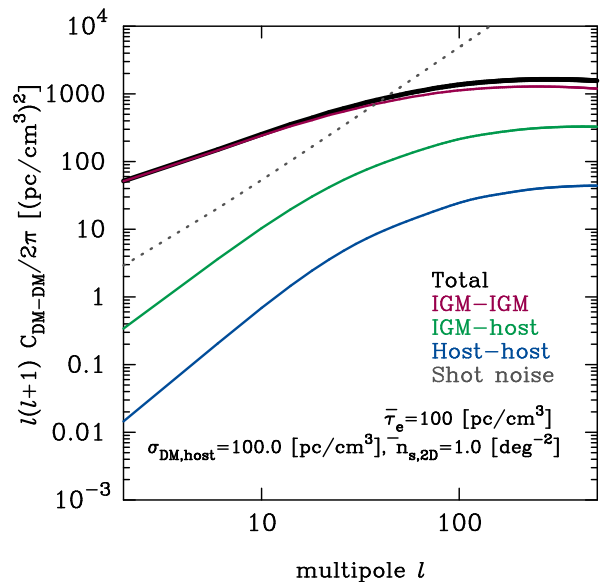


FIG. 1. Auto power spectrum of dispersion measure (DM). Colored lines represent contributions from the autocorrelation of the IGM component (red), the cross-correlation of the IGM and host-galaxy components (green), and autocorrelation of the host-galaxy component (blue). The solid black line shows the total power. The mean DM around host galaxies $\bar{\tau}_e$ is set to be 100 pc cm^{-3} . The dashed gray line indicates the shot noise induced by the intrinsic scatter of DM around host galaxies $\sigma_{\text{DM,host}}$. Here we assume the average source number density of $\bar{n}_{s,2\text{D}} = 1 \text{ deg}^{-2}$ and $\sigma_{\text{DM,host}} = 100 \text{ pc cm}^{-3}$.

Sample	Redshift range	$\bar{n}_g (h/\text{Mpc})^3$	Galaxy bias b_g
LOW-Z	$0.15 < z < 0.43$	3×10^{-4}	1.7
CMASS	$0.43 < z < 0.70$	3×10^{-4}	1.9
eBOSS	$0.70 < z < 1.60$	3×10^{-4}	1.3

TABLE I. Summary of galaxy samples assumed in this paper. The galaxy bias of LOW-Z and CMASS are found to be consistent with the previous works in Refs [39, 40].

sources and IGM, but they will be degenerate. We here consider cross-correlation analysis with galaxies in order to put additional constraints.

In general, galaxies trace the large-scale structure in a biased manner. The bias factor depends on the type of galaxies. Thus, the host galaxies of FRBs and their redshift evolution can be statistically inferred from spatial cross-correlation between FRBs and galaxies. A similar idea has been proposed in Ref [38] to constrain the redshift-distance relation of gravitational-wave sources. In principle, the three-dimensional information can be extracted from observables of FRBs alone; Ref [26] proposes that DMs can be used as the distance indicator as similar to redshift.

Let us consider a spectroscopic sample of galaxies with redshift ranging from $z_{i,\text{min}} < z < z_{i,\text{max}}$. The over-

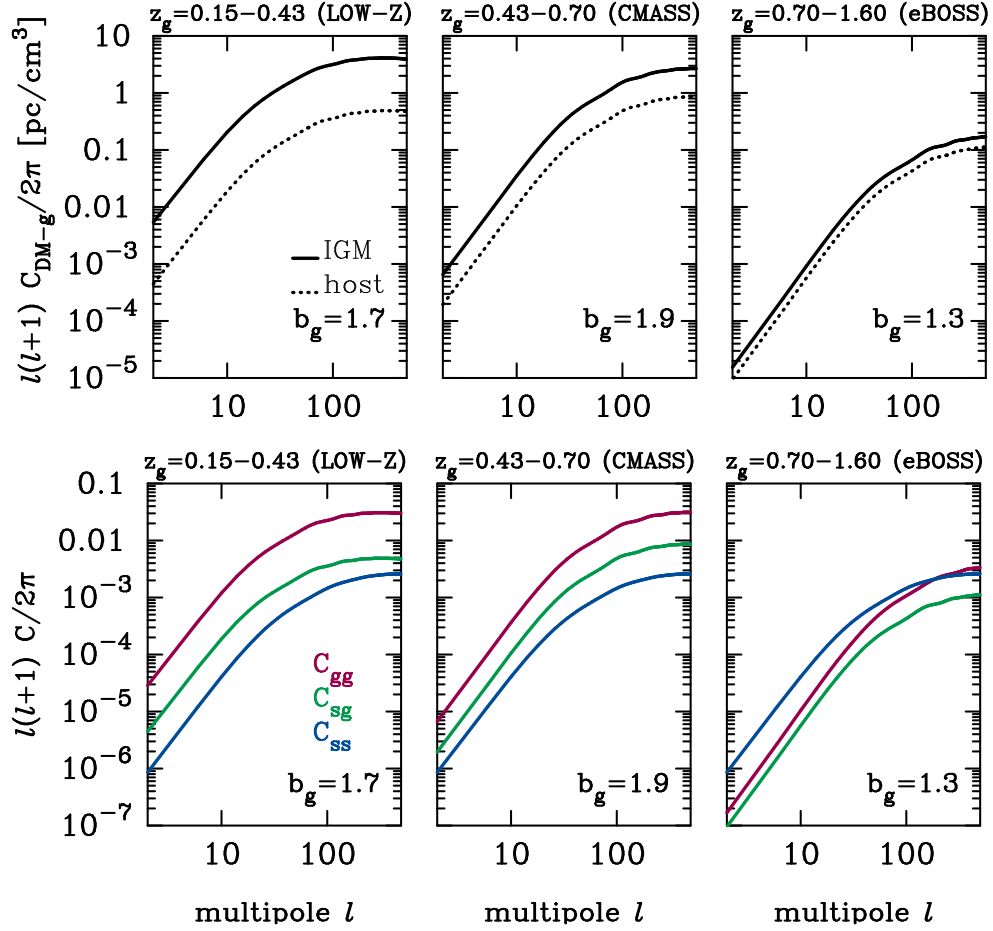


FIG. 2. Cross power spectra of FRB observables and galaxies. The upper panels show the cases for dispersion measures. The solid and dotted lines correspond to the contribution from the IGM and host galaxies, respectively. The bottom panels show the cases for angular number density of FRBs (green lines). We also show the auto power spectra of FRBs (blue lines) and galaxies (red lines) for comparison. Note that the similar shape among cross power spectra is expected in the linear bias model. In the linear bias model, the distribution of the relevant field such as electron number density is assumed to follow the matter density field.

density field of galaxies is expressed [in a similar way to Eq. (3)] as

$$\delta_{g,2D}^i(\boldsymbol{\theta}) = \int_0^\infty dz W_{g,i}(z) \delta_{g,i}(\boldsymbol{\theta}, z), \quad (28)$$

where $\delta_{g,i}$ represents the three-dimensional over-density field of galaxies. The window function $W_{g,i}(z)$ is

$$W_{g,i}(z) = \frac{1}{\bar{n}_{g,2D}^i} \frac{\chi^2}{H(z)} \bar{n}_g(z) \times \mathcal{H}(z - z_{i,\max}) \mathcal{H}(z_{i,\min} - z), \quad (29)$$

where $\bar{n}_g(z)$ is the average comoving number density of galaxies, $\mathcal{H}(x)$ is the Heaviside function, and $\bar{n}_{g,2D}^i = \int_{z_{i,\min}}^{z_{i,\max}} dz \chi^2 \bar{n}_g(z) / H(z)$.

Using the Limber approximation [35], the cross power spectrum of $\delta_{g,2D}^i$ and $\delta_{s,2D}$ can be given as

$$C_{sg,i}(\ell) = \int dz W_s(z) W_{g,i}(z) \frac{H(z)}{\chi^2(z)}$$

$$\times b_{\text{FRB}} b_{g,i} P_m \left(\frac{\ell + 1/2}{\chi}, z \right), \quad (30)$$

where we assume linear bias of $\delta_{g,i}(\boldsymbol{\theta}, z) = b_{g,i} \delta_m(\boldsymbol{\theta}, z)$. For each galaxy sample (identified by the index i), the correlation arises from the clustering in a finite redshift range of $z_{i,\min} < z < z_{i,\max}$. Therefore, $C_{sg,i}(\ell)$ contains the information of the source distribution $W_s(z)$. We can also compute the cross power spectrum of $\delta_{g,2D}^i$ and DM_{ext} as

$$C_{\text{DM-g},i} = C_{\text{IGM-g},i} + C_{\text{host-g},i}, \quad (31)$$

where

$$C_{\text{IGM-g},i} = \int dz W_{\text{DM,IGM}}(z) W_{g,i}(z) \frac{H(z)}{\chi^2(z)} \times b_e b_{g,i} P_m \left(\frac{\ell + 1/2}{\chi}, z \right), \quad (32)$$

$$C_{\text{host-g},i} = \int dz W_{\text{DM,host}}(z) W_{g,i}(z) \frac{H(z)}{\chi^2(z)}$$

$$\times b_{\text{FRB}} b_{g,i} P_m \left(\frac{\ell + 1/2}{\chi}, z \right), \quad (33)$$

which also contains the information of source distribution $W_s(z)$. Moreover, the mean DM from host galaxies $\bar{\tau}_e$ and the linear bias of sources b_{FRB} can be inferred from these power spectra.

In this paper, we consider three spectroscopic samples of galaxies from SDSS. These include two samples from the SDSS-III Baryon Oscillation Spectroscopic Survey (BOSS), named LOW-Z and CMASS [41]. We also consider emission-line galaxies to be catalogued by the SDSS-IV extended Baryonic Oscillation Spectroscopic Survey (eBOSS) [42]. The characteristics of these samples are summarized in Table I.

Fig. 2 shows the expected cross power spectra. We assume $b_{\text{FRB}} = 1.3$, $b_e = 1$, and $\bar{\tau}_e = 100 \text{ pc cm}^{-3}$ as in Figure 1. For both $C_{sg,i}$ and $C_{\text{DM}-g,i}$, the highest redshift bin has the smallest power. This is because we set an exponential cutoff for the FRB source distribution as $z_{\text{cut}} = 0.5$ (see Eq. 5). When the mean DM from host galaxies is set to be 100 pc cm^{-3} , the contribution from IGM is dominant in the range of $0.15 < z < 0.70$, while the contribution from host galaxies can become important at $z > 0.70$. We note that the contribution from IGM is proportional to the integration term $\int_z^\infty dz W_s(z)$ that is decreasing quickly for higher redshift in the presence of the exponential cutoff as in Eq. (5).

D. Signal-to-noise ratio

The S/N of angular power spectrum essentially determines to what extent we can extract source information from the clustering analysis. For given multiple field X and Y , the S/N of cross power spectrum $C_{XY}(\ell)$ can be computed as

$$\left[\frac{S}{N} \right]^2 (\ell_{\text{max}}) = \sum_{\ell_i, \ell_j < \ell_{\text{max}}} \text{Cov}_{XY}^{-1}[\ell_i, \ell_j] \times C_{XY}(\ell_i) C_{XY}(\ell_j), \quad (34)$$

where $\text{Cov}_{XY}[\ell_i, \ell_j]$ represents the covariance matrix between two modes of ℓ_i and ℓ_j . We assume that all the observable fields follow Gaussian distribution. This is reasonable since our primary focus is on large-scale modes ($\gtrsim 1 \text{ deg}$) for which the linear perturbation theory gives accurate results. For Gaussian fields X and Y , the covariant matrix is described as

$$\text{Cov}_{XY}[\ell_i, \ell_j] = \frac{\delta_{ij}}{(2\ell_i + 1)\Delta\ell f_{\text{sky}}} \left[C_{\text{obs},XX}(\ell_i) C_{\text{obs},YY}(\ell_i) + C_{\text{obs},XY}^2(\ell_i) \right], \quad (35)$$

where f_{sky} is the observed sky fraction. We consider binned power spectra with a bin width of $\Delta\ell$. In Eq. (35), the observed spectra of $C_{\text{obs},XX}$, $C_{\text{obs},YY}$ and $C_{\text{obs},XY}$ include both clustering signal and shot noise. We consider

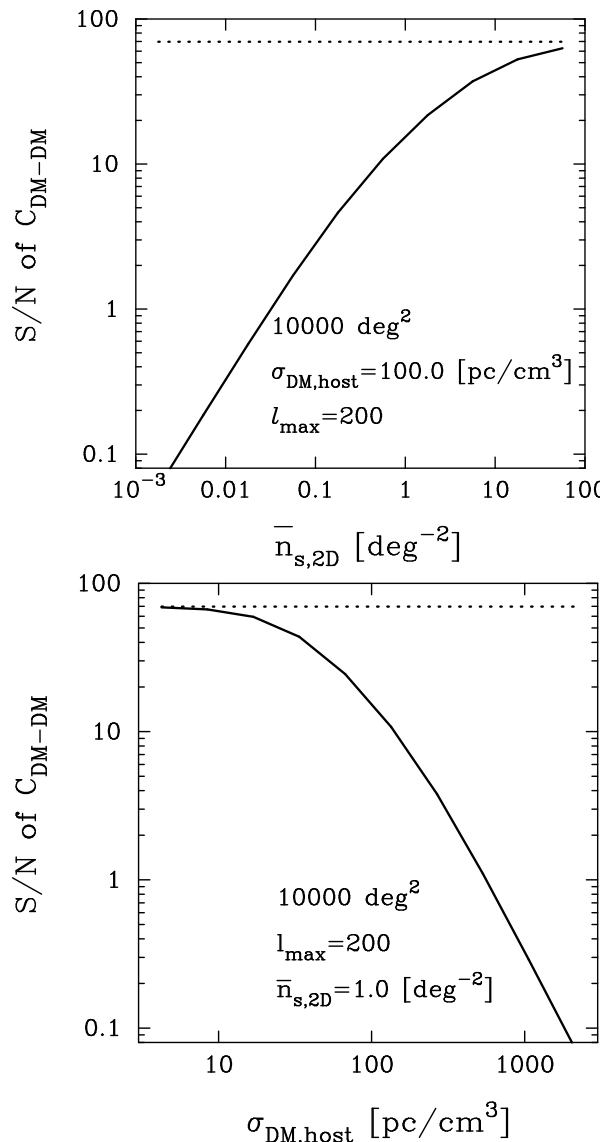


FIG. 3. Signal-to-noise ratio (S/N) of the autocorrelation of DMs. In the top panel, we plot the S/N as a function of the average source number density $\bar{n}_{s,2D}$ for a fixed intrinsic scatter of DM around host galaxies, $\sigma_{\text{DM,host}} = 100 \text{ pc cm}^{-3}$. In the bottom panel, we plot the S/N as a function of $\sigma_{\text{DM,host}}$ for $\bar{n}_{s,2D} = 1 \text{ deg}^{-2}$. In both, we set the maximum multipole to be $l_{\text{max}} = 200$ and assume a sky coverage of $10,000 \text{ deg}^2$. The dotted lines in both panels represent the case in the absence of the shot noise (i.e., $\sigma_{\text{DM,host}} = 0 \text{ pc cm}^{-3}$).

three fields, $\delta_{s,2D}$, DM_{est} , and $\delta_{g,2D}^i$, and then calculated the observed spectra as follows:

$$C_{\text{obs},ss}(\ell) = C_{ss}(\ell) + \frac{1}{\bar{n}_{s,2D}} \quad (36)$$

$$C_{\text{obs},\text{DM-DM}}(\ell) = C_{\text{DM-DM}}(\ell) + \frac{\sigma_{\text{DM,host}}^2}{\bar{n}_{s,2D}}, \quad (37)$$

$$C_{\text{obs},gi-gj}(\ell) = \delta_{ij} \left[C_{gg,i}(\ell) + \frac{1}{\bar{n}_{g,2D}} \right], \quad (38)$$

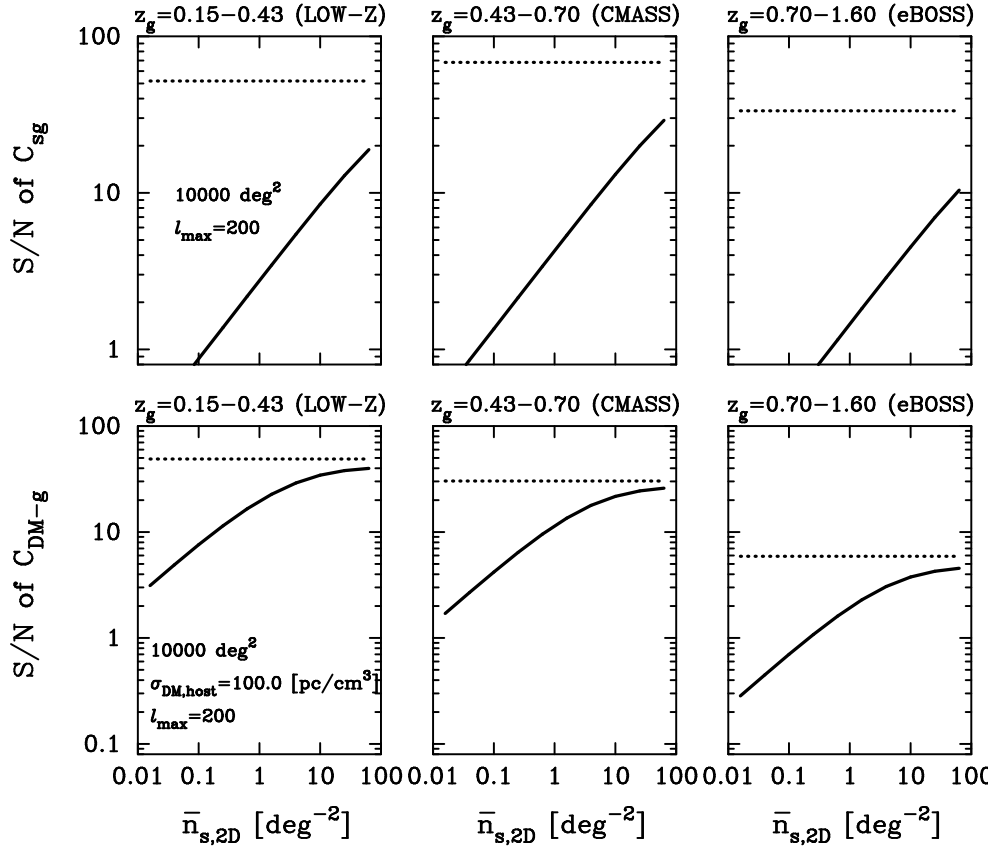


FIG. 4. S/N of the cross-correlation of FRBs and three spectroscopic galaxy samples as a function of the average source number density of FRBs. The top and bottom panels show the S/N of $C_{sg,i}$ and $C_{DM-g,i}$, respectively. In the bottom panels, we assume the intrinsic scatter of DM to be $\sigma_{DM,host} = 100 \text{ pc cm}^{-3}$. The dotted lines represent the case with $\sigma_{DM,host} = 0$ and $\bar{n}_{s,2D} \rightarrow \infty$.

$$C_{\text{obs},sg,i}(\ell) = C_{sg,i}(\ell), \quad (39)$$

$$C_{\text{obs},DM-g,i}(\ell) = C_{DM-g,i}(\ell). \quad (40)$$

Autocorrelation of dispersion measures

The definitions of C_{ss} , C_{DM-DM} , $C_{sg,i}$, and $C_{DM-g,i}$ are shown in Secs. II B and II C, and the galaxy spectrum is defined as

$$C_{gg,i}(\ell) = \int dz W_{g,i}^2(z) \frac{H(z)}{\chi^2(z)} \times b_{g,i}^2 P_m \left(\frac{\ell + 1/2}{\chi}, z \right). \quad (41)$$

Note that the shot noise is absent in the cross-correlation analysis. In the following, we set the survey area to be $10,000 \text{ deg}^2$, which roughly corresponds to the area of SDSS. We set $\ell_{\text{max}} = 200$, $\ell_{\text{min}} = 10$ and $\Delta\ell = 50$ as constant and investigate the clustering signals of scales larger than $2\pi/\ell_{\text{max}} = 1.8 \text{ deg}$. Following results are not sensitive to the choice of $\Delta\ell$ since the power spectra have simple shapes as shown in Figures 1 and 2.

We first consider the autocorrelation of DMs. We here adopt our fiducial model of $C_{DM-DM}(\ell)$ as shown in Fig. 1. We then examine the effect of shot noise on the detectability of the clustering signal.

The top panel in Fig. 3 shows the S/N of C_{DM-DM} for various average source number densities. For an intrinsic scatter of $\sigma_{DM,host} = 100 \text{ pc cm}^{-3}$, the clustering signal can be identified with a 5σ significance by detecting ~ 1000 FRBs. Once $10,000$ FRBs are observed, the S/N can be ~ 10 , corresponding to a measurement of C_{DM-DM} with a $\sim 10\%$ accuracy. The effect of $\sigma_{DM,host}$ on the detectability of C_{DM-DM} is shown in the bottom panel where we assume $10,000$ FRBs are observed in a $10,000 \text{ deg}^2$ field. According to this figure, we can measure C_{DM-DM} with a $10 - 20\%$ accuracy even if $\sigma_{DM,host}$ is of an order of 100 pc cm^{-3} .

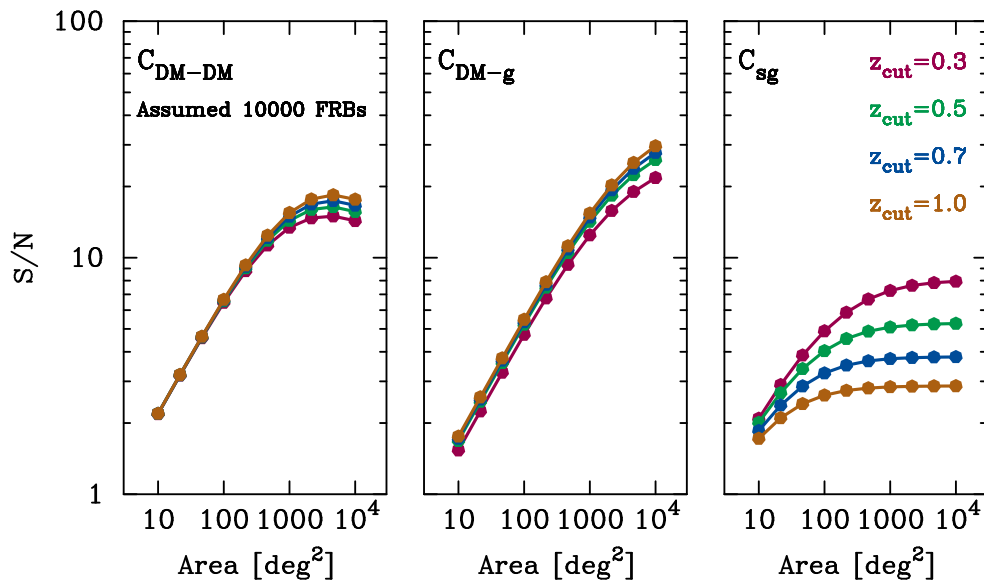


FIG. 5. Dependence of the S/N of FRB clustering signals on the survey parameters. In each panel, different color lines represent the different values of redshift cutoff z_{cut} in Eq (5), corresponding to different detection thresholds of radio survey. We set the maximum multipole as $\ell_{\text{max}} = 200$ and the intrinsic scatter of DM as $\sigma_{\text{DM,host}} = 100 \text{ pc cm}^{-3}$. The left, medium, and right panels show the cases of autocorrelation of DMs ($C_{\text{DM-DM}}$), cross-correlation of DMs and galaxies ($C_{\text{DM-g}}$), and cross-correlation of positions between sources and galaxies (C_{sg}), respectively.

Cross-correlation with galaxy distribution

We next consider the cross-correlation with galaxy distribution. When computing the S/N, we adopt the fiducial model as shown in Fig. 2. Fig. 4 summarizes the S/N of cross power spectra as a function of average source number density.

The upper panels show the cases of cross-correlation between FRB sources and galaxies, while the bottom panels are for the correlation between DMs and galaxies. Compared with the autocorrelation (Fig. 3), we require a larger number of events to detect the clustering signals; 10,000 events are necessary to detect C_{sg} for LOW-Z and CMASS samples with a $\sim 3\sigma$ significance, whereas it is difficult to detect the signal for the highest redshift bin. We also find that the shot noise will dominate for average source number density of $\bar{n}_{\text{s,2D}} < 10 \text{ deg}^{-2}$.

The bottom panels show that the S/N of $C_{\text{DM-g}}$ can be close to the cosmic-variance limit with 10,000 FRBs in the $10,000 \text{ deg}^2$ field, resulting in the measurement with a $\sim 5 - 10\%$ accuracy for LOW-Z and CMASS samples and $\sim 50\%$ accuracy for eBOSS sample. The effect of $\sigma_{\text{DM,host}}$ on the detectability of $C_{\text{DM-host}}$ is similar to the case of $C_{\text{DM-DM}}$ (Fig. 3 bottom). The S/N will be degraded by a factor of 3 – 5 when we increase $\sigma_{\text{DM,host}}$ from 20 pc cm^{-3} to 100 pc cm^{-3} .

We should note that a measurement of C_{sg} with a 5% accuracy roughly leads to constrain $b_{\text{FRB}}W_{\text{s}}(z_{\text{g}})$ with a similar accuracy where z_{g} represents the redshift of a given galaxy sample (see also Eq. 30). Likewise a measurement of $C_{\text{DM-g}}$ with a 5% accuracy constrains

$b_{\text{e}}W_{\text{DM,IGM}}(z_{\text{g}})$ with a $\sim 5\%$ accuracy.

Dependence on the FRB survey configuration

So far we consider a specific detection threshold in FRB clustering analyses. In our theoretical framework shown in Sec. II, the redshift cutoff z_{cut} in Eq (5) represents the detection threshold of the FRB survey; a smaller z_{cut} corresponds to a lower sensitivity. Radio surveys can be roughly categorized into two types: (i) a low detection threshold with a large sky coverage and (ii) a high detection threshold with a small sky coverage. The former corresponds to “imaging” survey, while the latter is “beam-formed” survey. Here we calculate the S/N of FRB clustering signals as a function of the total survey area and z_{cut} in order to demonstrate which survey strategy (beam-formed or imaging) will be suitable.

Fig. 5 summarizes the S/N of three clustering analyses $C_{\text{DM-DM}}$, $C_{\text{DM-g}}$, and C_{sg} as a function of the total area and z_{cut} . In this figure, we assume 10,000 detections and adopt the fiducial model of clustering signals. For cross-correlation analyses of $C_{\text{DM-g}}$ and C_{sg} , we properly combine three redshift bins of galaxies that are given by Table I. In general, a larger sky coverage improves the S/N more efficiently and the effects of the cutoff z_{cut} are not significant. This is simply because the statistical uncertainty of the clustering analyses scales with inverse of survey area. Although a hypothetical survey with a larger source number density in the same sky coverage can suppress the shot noise in clustering signals, the sta-

Analysis	Parameters of interest	Physical meaning	Fiducial value
$C_{\text{DM-DM}}, C_{\text{DM-g}}$	b_e	The fraction of free electrons in the unit of 0.88	1
$C_{\text{DM-DM}}, C_{\text{DM-g}}$	$b_{\text{FRB}} \bar{\tau}_e$	The bias of sources times mean DM around source population	$1.3 \times 100 \text{ pc cm}^{-3}$
C_{s_g}	b_{FRB}	The bias of sources	1.3
$C_{\text{DM-DM}}, C_{\text{DM-g}}, C_{s_g}$	$W_s(z)$	The redshift distribution of sources of FRBs	Eq (5)

TABLE II. Set of parameters that will be constrained by large-scale clustering of FRBs. In principle, the autocorrelation of source number density field C_{ss} should also contain some information of $W_s(z)$ and b_{FRB} . However, it is expected to be difficult to detect the signal from C_{ss} even with $\sim 10,000$ FRBs.

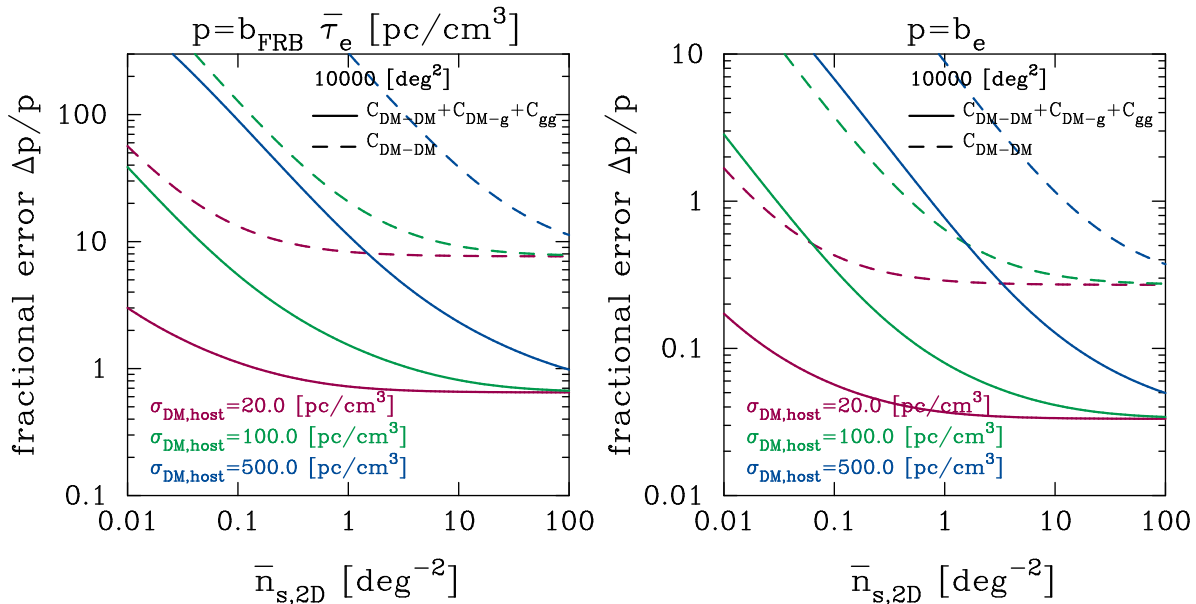


FIG. 6. Fractional errors of parameters as a function of average source number density and intrinsic scatter of DM around host galaxies $\sigma_{\text{DM,host}}$. The left panel shows the case for $b_{\text{FRB}} \bar{\tau}_e$ and the right is for b_e . In both panels, the dashed lines represent the constraints only from the auto-correlation of DMs and the solid lines are for the combined analysis with the cross correlation with galaxy distribution. The color difference corresponds to the difference of $\sigma_{\text{DM,host}}$: 20 pc cm^{-3} in red, 100 pc cm^{-3} in green and 500 pc cm^{-3} in blue.

tistical uncertainty will always dominate.

The effects of z_{cut} will appear in the clustering signals of $C_{\text{DM-DM}}$ and $C_{\text{DM-g}}$ only when the sky coverage will be close to $\sim 10,000$ squared degrees. This is because that $C_{\text{DM-DM}}$ and $C_{\text{DM-g}}$ is mainly determined by low-redshift structures. According to the left and medium panels, the S/N of $C_{\text{DM-DM}}$ and $C_{\text{DM-g}}$ will vary from ~ 10 to ~ 20 for $z_{\text{cut}} = 0.3 - 1.0$. This suggests that the difference of z_{cut} will induce a $\sim 1/20 - 1/10 \sim 5\%$ effect on the clustering signals. It should be noted that the S/Ns converge for $z_{\text{cut}} \gtrsim 0.5$.

The S/N of C_{s_g} will be affected by z_{cut} when the sky coverage is larger than ~ 100 squared degrees. The statistical uncertainty of C_{s_g} is mainly determined by the poisson term (source number density) when 10,000 detections are assumed. Among the galaxy samples in Table I, LOW-Z and CMASS contribute the most to the signal of C_{s_g} since the structures at lower-redshift have a larger clustering amplitude at degree scales. We find that low-

ering z_{cut} can improve the S/N of C_{s_g} more efficiently. For example, with a sky coverage of 10,000 square degrees, the S/N of C_{s_g} with $z_{\text{cut}} = 0.3$ is larger than that with $z_{\text{cut}} = 1.0$ by a factor of ~ 3 .

From the above results, we conclude that future imaging surveys with $z_{\text{cut}} \sim 0.5$ and a larger sky coverage as possible are suitable for large-scale clustering analyses of FRBs.

III. PARAMETER CONSTRAINTS

In Sec. IID, we show that $\sim 10,000$ FRBs over the sky coverage of $\sim 10,000 \text{ deg}^2$ will enable to detect the large-scale clustering signals of FRBs with a high S/N. Here we investigate what we can learn from such precise measurements. We perform a Fisher analysis of the FRB autocorrelation and the cross-correlation with SDSS galaxies in order to quantify the constraints on the model

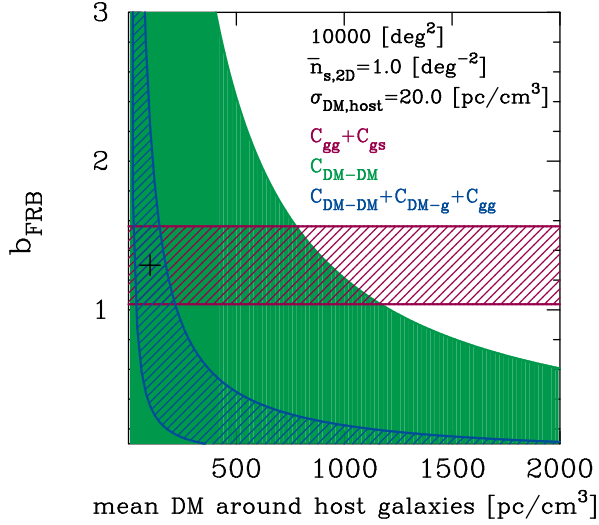


FIG. 7. The expected constraint in $\bar{\tau}_e - b_{\text{FRB}}$ plane. The green filled region shows the 68% confidence region from $C_{\text{DM-DM}}$ alone, while the blue hatched region represents the 68% confidence region from the combined analysis with C_{gg} , $C_{\text{DM-g}}$ and $C_{\text{DM-DM}}$. The red is for the combined analysis with C_{gg} and C_{gs} . In this figure, we assume 10,000 events with the sky coverage of 10,000 deg^2 and the intrinsic scatter of DM around host $\sigma_{\text{DM,host}} = 20 \text{ pc cm}^{-3}$.

parameters. The details of our Fisher analysis are summarized in Appendix A and the parameters of interest are shown in Table II³.

Fig. 6 shows the dependence of the determination accuracy of $b_{\text{FRB}}\bar{\tau}_e$ and b_e with respect to $\bar{n}_{s,2D}$ and $\sigma_{\text{DM,host}}$. We find that one can determine b_e with an uncertainty of 30-1000% by $C_{\text{DM-DM}}$ alone with $\sim 10,000$ FRBs (dashed lines in the right panel). On the other hand, $C_{\text{DM-DM}}$ will not put a meaningful constraint on $b_{\text{FRB}}\bar{\tau}_e$ if the IGM contribution is dominant as in our fiducial model (dashed lines in the left panel). Importantly, by combining the cross correlation $C_{\text{DM-g}}$ and C_{gg} , the constraints on $b_{\text{FRB}}\bar{\tau}_e$ and b_e can be significantly improved by a factor of ~ 10 for a wide range of $\bar{n}_{s,2D}$ and $\sigma_{\text{DM,host}}$ (solid lines).

Only using $C_{\text{DM-DM}}$, $C_{\text{DM-g}}$ and C_{gg} , the constraints on b_{FRB} and $\bar{\tau}_e$ are strongly degenerate. This degeneracy is resolved by adding C_{gs} as demonstrated in Fig. 7. With 10,000 FRBs in the 10,000 deg^2 field and $\sigma_{\text{DM,host}} = 20 \text{ pc cm}^{-3}$, the fractional error of b_{FRB} and

$\bar{\tau}_e$ can become as small as $\sim 20\%$ and $\sim 70\%$, respectively. More generally, the fractional errors of b_{FRB} and $b_{\text{FRB}}\bar{\tau}_e$ are approximately given as

$$\frac{\Delta b_{\text{FRB}}}{b_{\text{FRB}}} \simeq 0.2 \left(\frac{\bar{n}_{s,2D}}{1 \text{ deg}^{-2}} \right)^{-0.5}, \quad (42)$$

$$\frac{\Delta(b_{\text{FRB}}\bar{\tau}_e)}{b_{\text{FRB}}\bar{\tau}_e} \simeq 0.7x^2 \left\{ 0.05 \left(\frac{\sigma_{\text{DM,host}}}{20.0 \text{ pc cm}^{-3}} \right)^{-0.3} + 1/x^2 \right\}, \quad (43)$$

where x in Eq. (43) is defined as

$$x = \left(\frac{\sigma_{\text{DM,host}}}{20.0 \text{ pc cm}^{-3}} \right) \left(\frac{\bar{n}_{s,2D}}{1 \text{ deg}^{-2}} \right)^{-1/2}. \quad (44)$$

Note that the bias factor of star-forming galaxies and passive galaxies at $z < 1$ are $b_{\text{FRB}} = 1.3$ and $= 1.7 - 1.9$, respectively [43] and the difference is also $\sim 20\%$. Thus, the host galaxy type of FRBs can be statistically inferred once $\sim 10,000$ FRBs are detected in the 10,000 deg^2 field.

So far we have assumed that the FRB source distribution follows the star-formation history (Eqs. 5 and 6). Since $C_{\text{DM-DM}}$, $C_{\text{DM-g}}$ and C_{sg} contain information of W_s [Eqs. (22), (30), and (32)], the redshift distribution of FRB sources can be also constrained from the clustering analysis, in principle. As a representative example, we here consider a time delay distribution $f(\Delta t) \propto (\Delta t)^{-\alpha_t}$ with $\Delta t > 20 \text{ Myr}$. For a given α_t , we can compute the source distribution by convoluting the delay time distribution and the global star-formation history:

$$\bar{n}_{s,\text{delay}}(z; \alpha_t) = \mathcal{A} \exp \left[-\frac{d_L^2(z)}{2d_L^2(z_{\text{cut}})} \right] \times \int_z^\infty dz' \dot{\rho}_*(z'; \alpha_1 = 0.13) \times \left(\frac{t(z) - t(z')}{\Delta t_{\text{norm}}} \right)^{-\alpha_t} \frac{dt}{dz'} \quad (45)$$

where $t(z)$ is the age of universe as a function of z , Δt_{norm} is the normalization factor for the delay time distribution and $\dot{\rho}_*(z)$ is given by Eq. (6). By comparing our fiducial model [Eq. (5)] and $\bar{n}_{s,\text{delay}}(z; \alpha_t)$, we find the approximated correspondence between two models: $\alpha_t = 0.5$ in Eq. (45) corresponds to $\alpha_1 = 0$ in Eq. (5), while $\alpha_t = 1.0$ in Eq. (45) is for $\alpha_1 = 0.2 \times 0.13$ in Eq. (5).

We find that the fractional error of α_1 scales as

$$\frac{\Delta \alpha_1}{\alpha_1} \simeq 4.0 \left(\frac{\bar{n}_{s,2D}}{1 \text{ deg}^{-2}} \right)^{-0.5}, \quad (46)$$

with $C_{sg} + C_{gg}$ for the sky coverage of 10,000 deg^2 . Eq (46) shows that we require $\gtrsim 160,000$ events on 10,000 deg^2 to constrain on $\alpha_t < 0.5$, whereas 4×10^6 events enable us to constrain on $\alpha_t < 1$. It should be noted that the model of $\alpha_t = 1$ roughly corresponds to the neutron-star merger scenario [44].

³ It's worth mentioning that the forecast in the Fisher analysis depends on the choice of fiducial value of the parameters in principle. Nevertheless, the expected error in FRB parameters is found to be less affected by the choice of fiducial value if we set $\bar{n}_{s,2D} \simeq 1 \text{ deg}^{-2}$ and $\sigma_{\text{DM,host}} \simeq 100 \text{ pc cm}^{-3}$. This is because the statistical uncertainty of clustering signals is mainly determined by the Poisson noise in our case and the clustering signal is assumed to be proportional to the parameters of b_e , b_{FRB} and $b_{\text{FRB}}\bar{\tau}_e$.

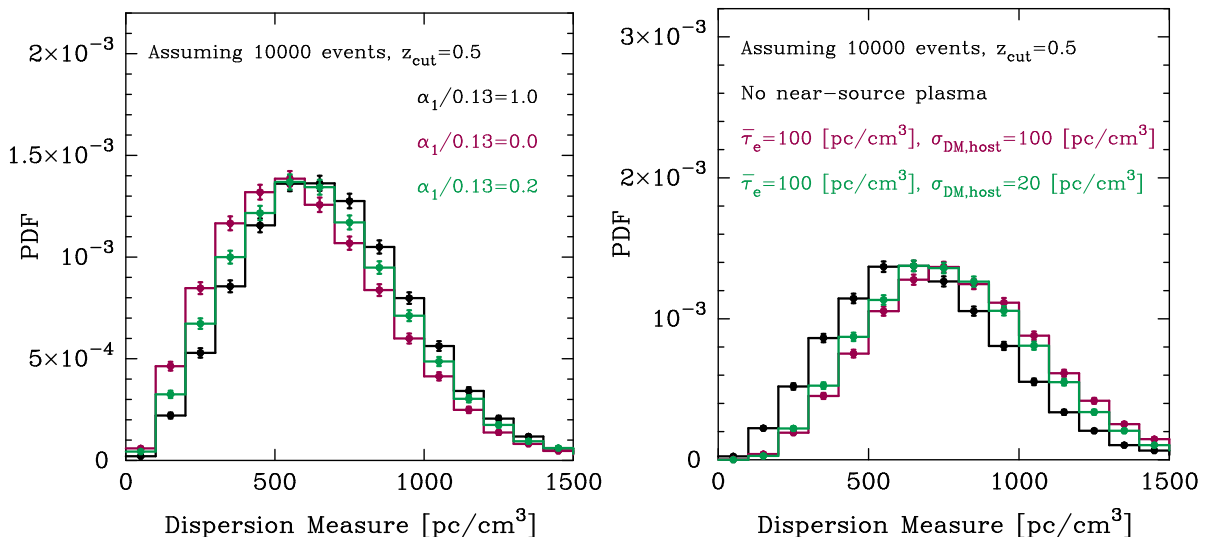


FIG. 8. Dependence of the probability distribution function (PDF) of observed DM on FRB source distribution (left) and DM around host galaxies (right). In both panels, the black line shows our fiducial case with a source distribution of Eq. (5) and $\bar{\tau}_e = 0$. The colored lines in left panel represent the model PDF with different values of α_1 [Eq. (5)]. The red and green lines in right panel show the cases with $\bar{\tau}_e = 100$ pc cm⁻³ and $\sigma_{\text{DM,host}} = 100$ pc cm⁻³ or 20 pc cm⁻³, respectively. The error bars in both panels show the poisson error for 10,000 events.

A. Combining DM distribution function

As shown in the previous section, even 10,000 FRBs are not enough to obtain meaningful constraints on the redshift distribution of FRB sources if we only use the large-scale clustering. In order to improve the constraint, we need additional information other than two-point correlation functions.

One of the simplest FRB statistics is one-point distribution function or probability distribution function (PDF) of DM. It is suggested that the DM PDF contains rich cosmological information [23]. For example, Ref. [45] proposes to use the DM PDF to determine the formation mechanism of FRBs. Here we explore how the constraint on the redshift distribution of FRB sources can be improved by combining the DM PDF.

The left panel of Fig. 8 shows the DM PDFs with different source redshift distributions⁴. The black line shows our fiducial model with $\alpha_1 = 0.13$ in Eq. (5), while the red and green lines are for $\alpha_1 = 0$ and 0.13×0.2 , respectively. As expected, the mean value of DM becomes smaller for a larger delay time. The error bar in Fig. 8 represents the poisson error for 10,000 FRBs. The left panel clearly shows the statistical power of DM PDF to constrain the source redshift distribution. As in Sec. III, the model of $\alpha_t = 1$ roughly corresponds to the neutron-star merger scenario; the DM PDF of 10000 events is sufficient to constrain the various time-delayed models

in Eq (45). However, we should stress that in the left panel we neglect the contribution from DM_{host}, which in general affect the observed DM PDF.

The right panel in Fig. 8 shows the impact of DM_{host} on DM PDF. As for the PDF of DM_{host}, we assume that DM_{host} follows Gaussian distribution with mean of $\bar{\tau}_e$ and scatter of $\sigma_{\text{DM,host}}$. The black line in the right panel is the same as that in the left panel while the red and green lines correspond to the cases with $\bar{\tau}_e = 100$ pc cm⁻³ and $\sigma_{\text{DM,host}} = 100$ pc cm⁻³ or 20 pc cm⁻³, respectively. In the right panel, we set the source distribution as our fiducial model [Eq. (5)]. Of course, the mean value of DM becomes larger when including DM_{host}. One can see that the effects of $\sigma_{\text{DM,host}}$ will be minor as far as $\sigma_{\text{DM,host}} \lesssim \bar{\tau}_e$.

Fig. 8 shows that DM PDF is a powerful probe of the redshift distribution of FRB sources. Note, however, that expected constraints from DM PDF are dependent on the intrinsic properties of DM_{host}. Unfortunately, our result indicates that it is difficult to determine the source distribution and the mean host DM with PDF alone. In contrast, the large-scale clustering of FRBs has a good sensitivity for $\bar{\tau}_e$ and $\sigma_{\text{DM,host}}$. Therefore, by combining the large-scale clustering and PDF of FRBs, the redshift distribution of FRB sources can be also constrained with a similar accuracy to $\bar{\tau}_e$ in Figure 7. In order to study more detailed information content in the combined analysis, we require more accurate modeling of FRBs and leave it for our future work.

⁴ The details of our modeling of cosmological DM are summarized in Appendix B.

IV. CONCLUSION AND DISCUSSION

In this paper, we have studied the information content in large-scale clustering of FRBs at degree scales. We have developed a theoretical framework for the clustering analyses based on the standard theory of structure formation. In addition to the two-point clustering of FRB source number density and extragalactic DMs, we have considered the cross-correlation with galaxy distributions to identify the origin of FRBs. Assuming a reasonable parameter set, we have investigated the S/N of clustering signals and made a forecast for expected constraints on the model parameters obtained by future radio transient surveys. Our main findings are summarized as follows:

1. The autocorrelation of DMs consists of contributions from the clustering of IGM, the clustering of host galaxies, the clustering due to overlapped redshift distribution between IGM and host galaxies, and the shot noise originating from the intrinsic scatter of DM around host galaxies. Among these, the IGM clustering is likely to be dominant in the autocorrelation of DM_{ext} . The typical amplitude is expected to be $\sim 0.1\text{-}10 [\text{pc cm}^{-3}]^2$ in the range of $\ell \sim 10\text{-}200$. The clustering between IGM and host galaxies can be significant if the mean DM around host galaxies $\bar{\tau}_e$ is $\sim 600\text{-}700 \text{ pc cm}^{-3}$.
2. The S/N of autocorrelation of DMs depends on the average source number density $\bar{n}_{s,2D}$ and the intrinsic scatter of DM around host galaxies $\sigma_{\text{DM,host}}$ for a fixed survey area. Assuming a hypothetical survey with the sky coverage of $10,000 \text{ deg}^2$ and $\sigma_{\text{DM,host}} = 100 \text{ pc cm}^{-3}$, we estimate that 1,000 events are sufficient to detect the clustering signal of IGM with a 3σ significance. A sample of 10,000 FRBs enable us to measure the signal with a $\sim 10\%$ accuracy at degree scales. A similar S/N can be obtained in the cross-correlation of DMs and the galaxy distribution from existing spectroscopic galaxy samples. The cross-correlation of FRBs with galaxy distributions in the redshift range of $0.15 < z < 1.6$ can be detected with a $\gtrsim 3\sigma$ confidence level if $\sim 10,000$ FRBs are observed.
3. Measurement of large-scale clustering of FRBs can place constraints on the fraction of free electrons, the environment of the source population(s), and the mean DM around host galaxies. The DM autocorrelation can be used to constrain the global abundance of free electrons at $z < 1$ with a level of $\sim 70\%$, if 10,000 FRBs are observed over $10,000 \text{ deg}^2$ and the intrinsic scatter of DM is assumed to be $\sigma_{\text{DM,host}} = 100 \text{ pc cm}^{-3}$. The cross-correlation with galaxy distributions will improve the constraint by a factor of ~ 10 . The cross-correlation of FRBs and galaxy distributions will

help determining the linear bias of the source population b_{FRB} with a level of $\sim 20\%$. If we add the information from the DM-galaxy cross-correlation, it is possible to put a tight constraint on the mean DM around host galaxies by statistical analysis in future transient surveys (see Fig. 7).

Our clustering analysis can be useful to identify the origin of FRB. In some models, FRBs are associated with newborn or young compact stellar objects, e.g., fast-spinning pulsars or magnetars [12–14]. In this case, FRBs typically occur in star-forming galaxies and the bias factor will be $b_{\text{FRB}} \sim 1.3$. The first identified FRB host of FRB 121102 may belong to this group [19]. On the other hand, e.g., in the compact binary merger scenarios [15, 16], FRBs will preferentially occur in more evolved galaxies and the bias factor can range from $b_{\text{FRB}} = 1.7 - 1.9$. In a more exotic scenario, e.g., evaporation of primordial black holes [2], the bias factor could be $b_{\text{FRB}} \sim 1$. Such a difference of the bias factor can be distinguished by the clustering analysis once $\sim 10,000$ of FRBs are detected in a sky area of $\sim 10,000 \text{ deg}^2$. Another key to distinguish the FRB source candidates is the delay time distribution, which can be also constrained by the combined analysis of clustering and DM distribution function (see Fig. 8). Although high-precision localization of FRBs with long-baseline observatories is still the most robust way to probe physical properties of FRB host galaxies and near source regions, a drawback is the small detection efficiency due to the limited field-of-view. Our statistical approach only requires an angular resolution of $\sim \text{deg}$ and will be complementary and powerful once $\sim 100 - 1000$ of FRBs are detected annually.

ACKNOWLEDGMENTS

M. S. is supported by Research Fellowships of the Japan Society for the Promotion of Science (JSPS) for Young Scientists. N. Y. and K. K. acknowledge financial support from JST CREST. Numerical computations presented in this paper were in part carried out on the general-purpose PC farm at the Center for Computational Astrophysics, CfCA, of the National Astronomical Observatory of Japan.

Appendix A: Fisher Analysis

Let us briefly summarize the Fisher analysis. For a multivariate Gaussian likelihood, the Fisher matrix F_{ij} can be written as

$$F_{ij} = \frac{1}{2} \text{Tr} [A_i A_j + C^{-1} H_{ij}], \quad (\text{A1})$$

where $A_i = C^{-1} \partial C / \partial p_i$, $H_{ij} = 2(\partial \mu / \partial p_i)(\partial \mu / \partial p_j)$, C is the data covariance matrix, μ represents the assumed model, and p_i describes parameters of interest. The

Fisher matrix provides an estimate of the error covariance for two parameters as

$$\langle \Delta p_\alpha \Delta p_\beta \rangle = (F^{-1})_{\alpha\beta}, \quad (\text{A2})$$

where Δp_α represents the statistical uncertainty of parameter p_α .

In the present study, we consider only the second term in Eq. (A1). Because C is expected to scale inversely to the survey area, the second term will be dominant for a large area survey. We consider the following parameters to vary: $\mathbf{p} = \{b_{g,1}, b_{g,2}, b_{g,3}, b_{\text{FRB}}, \alpha_1, b_{\text{FRB}}\bar{r}_e, b_e\}$ where $b_{g,i}$ is the galaxy bias for i th spectroscopic sample given by Table I and α_1 controls the redshift dependence of $W_s(z)$ [also see Eq (6)]. The fiducial values of \mathbf{p} are set to be $\mathbf{p}_{\text{fid}} = \{1.7, 1.9, 1.3, 1.3, 0.13, 130 \text{ pc cm}^{-3}, 1\}$.

We construct the data vector \mathbf{D} from a set of binned spectra $C_{\text{DM-DM}}, C_{\text{DM-g}}, C_{gg}$ and C_{gs} as

$$\begin{aligned} D_i = \{ & C_{\text{DM-DM}}(\ell_1), \dots, C_{\text{DM-DM}}(\ell_{10}), \\ & C_{\text{DM-g},1}(\ell_1), \dots, C_{\text{DM-g},1}(\ell_{10}), \\ & C_{\text{DM-g},2}(\ell_1), \dots, C_{\text{DM-g},2}(\ell_{10}), \\ & C_{\text{DM-g},3}(\ell_1), \dots, C_{\text{DM-g},3}(\ell_{10}), \\ & C_{gg,1}(\ell_1), \dots, C_{gg,1}(\ell_{10}), \\ & C_{gg,2}(\ell_1), \dots, C_{gg,2}(\ell_{10}), \\ & C_{gg,3}(\ell_1), \dots, C_{gg,3}(\ell_{10}), \\ & C_{gs,1}(\ell_1), \dots, C_{gs,1}(\ell_{10}), \\ & C_{gs,2}(\ell_1), \dots, C_{gs,2}(\ell_{10}), \\ & C_{gs,3}(\ell_1), \dots, C_{gs,3}(\ell_{10})\}, \end{aligned} \quad (\text{A3})$$

where $\ell_i = \ell_{\text{min}} + (i + 0.5)(\ell_{\text{max}} - \ell_{\text{min}})/10$ with $\ell_{\text{min}} = 10$ and $\ell_{\text{max}} = 200$. The cross covariance between two spectra of C_{XY} and C_{AB} is then computed as

$$\begin{aligned} \text{Cov}_{XY,AB}[\ell_i, \ell_j] = & \frac{\delta_{ij}}{(2\ell_i + 1)\Delta\ell f_{\text{sky}}} \left[C_{\text{obs},XY}(\ell_i)C_{\text{obs},AB}(\ell_i) \right. \\ & \left. + C_{\text{obs},XA}(\ell_i)C_{\text{obs},YB}(\ell_i) \right], \end{aligned} \quad (\text{A4})$$

where the width is set to be $\Delta\ell = (\ell_{\text{max}} - \ell_{\text{min}})/10$ and we assume the sky fraction of $f_{\text{sky}} \simeq 10000/41252.96 = 0.242$.

Appendix B: Construction of mock FRB catalogs with cosmological N -body simulation

Here we summarize our modeling of DM_{IGM} based on cosmological N -body simulations. For DM_{IGM} , we as-

sume that the free-electron number density is an unbiased tracer of underlying matter density. In order to simulate the three-dimensional matter density distribution, we utilize a set of N -body simulations used in our previous work of Ref [46]. We employ 256^3 particles in a comoving volume of $240^3 [h^{-1} \text{ Mpc}]^3$ and damp ten snapshots in the redshift range of $z = 0 - 1$. We determine the output redshifts of simulation so that the simulation boxes are placed to cover a past light cone of a hypothetical observer with angular extent $5 \times 5 \text{ deg}^2$ from redshift $z = 0$ to $z \sim 1$. The details of our simulation are found in Ref [46].

From the distribution of N -body particles in each snapshot, we first generate three-dimensional matter density field on 256^3 grids by using the nearest-grid-point method. We then combine 10 grid-based density maps to generate a light cone outout with a line-of-sight depth of $\sim 2 \text{ Gpc}$. To avoid the same structure appearing multiple times along the line of sight, we randomly shift the simulation boxes. In total, we generate 20 quasi-independent realizations of matter density distribution in a comoving volume of $240 \times 240 \times 2400 [h^{-1} \text{ Mpc}]^3$. Note that the transverse grid size in the density maps corresponds to a few arcmin at $z \sim 0.5$. This is sufficient for upcoming wide-area FRB surveys such as CHIME.

We also locate dark matter halos using the standard friend-of-friend (FOF) algorithm with the linking parameter of $b = 0.2$. We then assume that FRBs occur in dark matter halos with the FOF mass greater than $10^{13} h^{-1} M_\odot$. Note that the mass selection of $> 10^{13} h^{-1} M_\odot$ roughly correspond to a sample with the halo bias of 1-1.5 [47]. Finally, we make a random down-sampling of halos so that the redshift distribution of FRB hosts can be approximated as assumed in our model. For the input redshift distribution of FRBs, we consider the functional form of Eq. (5) with $z_{\text{cut}} = 0.5$. As our fiducial model, we set $\alpha_0 = 0.0170$, $\alpha_1 = 0.13$, $\alpha_2 = 3.3$, and $\alpha_3 = 5.3$, while we examine a sensitivity of α_1 on DM PDF. After the random sampling, we find $\sim 2,000$ halos in each realization. For selected halos, we compute DM_{IGM} by summing the pixel value of grid-based matter density maps along the line of sight as in Eq. (8), assuming $\Omega_b h^2 = 0.022$ and $f_e = 0.88$.

-
- [1] D. R. Lorimer, M. Bailes, M. A. McLaughlin, D. J. Narkevic, and F. Crawford, *Science* **318**, 777 (2007), arXiv:0709.4301.
 [2] E. F. Keane, B. W. Stappers, M. Kramer, and A. G. Lyne, *Mon. Not. Roy. Astron. Soc.* **425**, L71 (2012),

arXiv:1206.4135 [astro-ph.SR].

- [3] D. Thornton, B. Stappers, M. Bailes, B. Barsdell, S. Bates, N. D. R. Bhat, M. Burgay, S. Burke-Spolaor, D. J. Champion, P. Coster, N. D'Amico, A. Jameson, S. Johnston, M. Keith, M. Kramer, L. Levin, S. Milia,

- C. Ng, A. Possenti, and W. van Straten, *Science* **341**, 53 (2013), arXiv:1307.1628 [astro-ph.HE].
- [4] S. Burke-Spolaor and K. W. Bannister, *Astrophys. J.* **792**, 19 (2014), arXiv:1407.0400 [astro-ph.HE].
- [5] L. G. Spitler, J. M. Cordes, J. W. T. Hessels, D. R. Lorimer, M. A. McLaughlin, S. Chatterjee, F. Crawford, J. S. Deneva, V. M. Kaspi, R. S. Wharton, B. Allen, S. Bogdanov, A. Brazier, F. Camilo, P. C. C. Freire, F. A. Jenet, C. Karako-Argaman, B. Knispel, P. Lazarus, K. J. Lee, J. van Leeuwen, R. Lynch, S. M. Ransom, P. Scholz, X. Siemens, I. H. Stairs, K. Stovall, J. K. Swiggum, A. Venkataraman, W. W. Zhu, C. Aulbert, and H. Fehrmann, *Astrophys. J.* **790**, 101 (2014), arXiv:1404.2934 [astro-ph.HE].
- [6] E. Petroff, M. Bailes, E. D. Barr, B. R. Barsdell, N. D. R. Bhat, F. Bian, S. Burke-Spolaor, M. Caleb, D. Champion, P. Chandra, G. Da Costa, C. Delvaux, C. Flynn, N. Gehrels, J. Greiner, A. Jameson, S. Johnston, M. M. Kasliwal, E. F. Keane, S. Keller, J. Kocz, M. Kramer, G. Leloudas, D. Malesani, J. S. Mulchaey, C. Ng, E. O. Ofek, D. A. Perley, A. Possenti, B. P. Schmidt, Y. Shen, B. Stappers, P. Tisserand, W. van Straten, and C. Wolf, *Mon. Not. Roy. Astron. Soc.* **447**, 246 (2015), arXiv:1412.0342 [astro-ph.HE].
- [7] V. Ravi, R. M. Shannon, and A. Jameson, *Astrophys. J. Letter* **799**, L5 (2015), arXiv:1412.1599 [astro-ph.HE].
- [8] K. Masui, H.-H. Lin, J. Sievers, C. J. Anderson, T.-C. Chang, X. Chen, A. Ganguly, M. Jarvis, C.-Y. Kuo, Y.-C. Li, Y.-W. Liao, M. McLaughlin, U.-L. Pen, J. B. Peterson, A. Roman, P. T. Timbie, T. Voytek, and J. K. Yadav, *Nature (London)* **528**, 523 (2015), arXiv:1512.00529 [astro-ph.HE].
- [9] D. J. Champion, E. Petroff, M. Kramer, M. J. Keith, M. Bailes, E. D. Barr, S. D. Bates, N. D. R. Bhat, M. Burgay, S. Burke-Spolaor, C. M. L. Flynn, A. Jameson, S. Johnston, C. Ng, L. Levin, A. Possenti, B. W. Stappers, W. van Straten, C. Tiburzi, and A. G. Lyne, *ArXiv e-prints* (2015), arXiv:1511.07746 [astro-ph.HE].
- [10] K. Ioka, *Astrophys. J.* **598**, L79 (2003), arXiv:astro-ph/0309200 [astro-ph].
- [11] S. Inoue, *Mon. Not. Roy. Astron. Soc.* **348**, 999 (2004), arXiv:astro-ph/0309364 [astro-ph].
- [12] S. B. Popov and K. A. Postnov, in *Evolution of Cosmic Objects through their Physical Activity*, edited by H. A. Harutyunian, A. M. Mickaelian, and Y. Terzian (2010) pp. 129–132, arXiv:0710.2006.
- [13] L. Connor, J. Sievers, and U.-L. Pen, *Mon. Not. Roy. Astron. Soc.* **458**, L19 (2016), arXiv:1505.05535 [astro-ph.HE].
- [14] Y. Lyubarsky, *Mon. Not. Roy. Astron. Soc.* **442**, L9 (2014), arXiv:1401.6674 [astro-ph.HE].
- [15] K. Kashiyama, K. Ioka, and P. Mészáros, *Astrophys. J. Letter* **776**, L39 (2013), arXiv:1307.7708 [astro-ph.HE].
- [16] T. Totani, *PASJ* **65**, L12 (2013), arXiv:1307.4985 [astro-ph.HE].
- [17] S. Chatterjee, C. J. Law, R. S. Wharton, S. Burke-Spolaor, J. W. T. Hessels, G. C. Bower, J. M. Cordes, S. P. Tendulkar, C. G. Bassa, P. Demorest, B. J. Butler, A. Seymour, P. Scholz, M. W. Abruzzo, S. Bogdanov, V. M. Kaspi, A. Keimpema, T. J. W. Lazio, B. Marcote, M. A. McLaughlin, Z. Paragi, S. M. Ransom, M. Rupen, L. G. Spitler, and H. J. van Langevelde, *Nature* **541**, 58 (2017).
- [18] B. Marcote, Z. Paragi, J. W. T. Hessels, A. Keimpema, H. J. van Langevelde, Y. Huang, C. G. Bassa, S. Bogdanov, G. C. Bower, S. Burke-Spolaor, B. J. Butler, R. M. Campbell, S. Chatterjee, J. M. Cordes, P. Demorest, M. A. Garrett, T. Ghosh, V. M. Kaspi, C. J. Law, T. J. W. Lazio, M. A. McLaughlin, S. M. Ransom, C. J. Salter, P. Scholz, A. Seymour, A. Siemion, L. G. Spitler, S. P. Tendulkar, and R. S. Wharton, *The Astrophysical Journal Letters* **834**, L8 (2017).
- [19] S. P. Tendulkar, C. G. Bassa, J. M. Cordes, G. C. Bower, C. J. Law, S. Chatterjee, E. A. K. Adams, S. Bogdanov, S. Burke-Spolaor, B. J. Butler, P. Demorest, J. W. T. Hessels, V. M. Kaspi, T. J. W. Lazio, N. Maddox, B. Marcote, M. A. McLaughlin, Z. Paragi, S. M. Ransom, P. Scholz, A. Seymour, L. G. Spitler, H. J. van Langevelde, and R. S. Wharton, *Astrophys. J. Letter* **834**, L7 (2017), arXiv:1701.01100 [astro-ph.HE].
- [20] C. J. Law, G. C. Bower, S. Burke-Spolaor, B. Butler, E. Lawrence, T. J. W. Lazio, C. A. Mattmann, M. Rupen, A. Siemion, and S. VanderWiel, *Astrophys. J.* **807**, 16 (2015), arXiv:1412.7536 [astro-ph.HE].
- [21] M. Caleb *et al.*, *Mon. Not. Roy. Astron. Soc.* **458**, 718 (2016), arXiv:1601.02444 [astro-ph.HE].
- [22] L. B. Newburgh *et al.*, *Proceedings, Ground-based and Airborne Telescopes VI: Edinburgh, United Kingdom, June 26-July 1, 2016*, *Proc. SPIE Int. Soc. Opt. Eng.* **9906**, 99065X (2016), arXiv:1607.02059 [astro-ph.IM].
- [23] M. McQuinn, *Astrophys. J.* **780**, L33 (2014), arXiv:1309.4451 [astro-ph.CO].
- [24] Y. Fujita, T. Akahori, K. Umetsu, C. L. Sarazin, and K.-W. Wong, *Astrophys. J.* **834**, 13 (2017), arXiv:1609.03566 [astro-ph.GA].
- [25] Z. Zheng, E. O. Ofek, S. R. Kulkarni, J. D. Neill, and M. Juric, *Astrophys. J.* **797**, 71 (2014), arXiv:1409.3244 [astro-ph.HE].
- [26] K. W. Masui and K. Sigurdson, *Phys. Rev. Lett.* **115**, 121301 (2015), arXiv:1506.01704 [astro-ph.CO].
- [27] P. A. R. Ade *et al.* (Planck), *Astron. Astrophys.* **594**, A13 (2016), arXiv:1502.01589 [astro-ph.CO].
- [28] S. Cole *et al.* (2dFGRS), *Mon. Not. Roy. Astron. Soc.* **326**, 255 (2001), arXiv:astro-ph/0012429 [astro-ph].
- [29] A. M. Hopkins and J. F. Beacom, *Astrophys. J.* **651**, 142 (2006), arXiv:astro-ph/0601463 [astro-ph].
- [30] E. Petroff, E. D. Barr, A. Jameson, E. F. Keane, M. Bailes, M. Kramer, V. Morello, D. Tabbara, and W. van Straten, (2016), 10.1017/pasa.2016.35, arXiv:1601.03547 [astro-ph.HE].
- [31] J. B. Muñoz, E. D. Kovetz, L. Dai, and M. Kamionkowski, *Phys. Rev. Lett.* **117**, 091301 (2016), arXiv:1605.00008 [astro-ph.CO].
- [32] J. H. Taylor and J. M. Cordes, *Astrophys. J.* **411**, 674 (1993).
- [33] W. Deng and B. Zhang, *Astrophys. J.* **783**, L35 (2014), arXiv:1401.0059 [astro-ph.HE].
- [34] R. K. Sheth and G. Tormen, *Mon. Not. Roy. Astron. Soc.* **308**, 119 (1999), astro-ph/9901122.
- [35] D. N. Limber, *Astrophys. J.* **119**, 655 (1954).
- [36] A. Lewis, A. Challinor, and A. Lasenby, *Astrophys. J.* **538**, 473 (2000), arXiv:astro-ph/9911177 [astro-ph].
- [37] C. Blake *et al.*, *Mon. Not. Roy. Astron. Soc.* **415**, 2876 (2011), arXiv:1104.2948 [astro-ph.CO].
- [38] M. Oguri, *Phys. Rev.* **D93**, 083511 (2016), arXiv:1603.02356 [astro-ph.CO].
- [39] M. Manera *et al.*, *Mon. Not. Roy. Astron. Soc.* **428**, 1036 (2012), arXiv:1203.6609 [astro-ph.CO].

- [40] M. Manera, L. Samushia, R. Tojeiro, C. Howlett, A. J. Ross, W. J. Percival, H. Gil-Marín, J. R. Brownstein, A. Burden, and F. Montesano, *Mon. Not. Roy. Astron. Soc.* **447**, 437 (2015), arXiv:1401.4171 [astro-ph.CO].
- [41] B. Reid *et al.*, *Mon. Not. Roy. Astron. Soc.* **455**, 1553 (2016), arXiv:1509.06529 [astro-ph.CO].
- [42] K. S. Dawson *et al.*, *Astron. J.* **151**, 44 (2016), arXiv:1508.04473 [astro-ph.CO].
- [43] I. Zehavi *et al.* (SDSS), *Astrophys. J.* **736**, 59 (2011), arXiv:1005.2413 [astro-ph.CO].
- [44] T. Piran, *Astrophys. J.* **389**, L45 (1992).
- [45] K. Dolag, B. M. Gaensler, A. M. Beck, and M. C. Beck, *Mon. Not. Roy. Astron. Soc.* **451**, 4277 (2015), arXiv:1412.4829 [astro-ph.CO].
- [46] M. Shirasaki, N. Yoshida, T. Hamana, and T. Nishimichi, *Astrophys. J.* **760**, 45 (2012), arXiv:1204.4981.
- [47] J. L. Tinker, B. E. Robertson, A. V. Kravtsov, A. Klypin, M. S. Warren, G. Yepes, and S. Gottlöber, *Astrophys. J.* **724**, 878 (2010), arXiv:1001.3162.